

# **Evaluation of Additively Manufactured Stacks for Thermoacoustic Devices**

Samarjith Biswas<sup>1</sup>
School of Mechanical and Aerospace Engineering, Oklahoma State University 201 General Academic Building, Stillwater, OK 74078

Zack Krawczyk<sup>2</sup>
School of Mechanical and Aerospace Engineering, Oklahoma State University 201 General Academic Building, Stillwater, OK 74078

James M. Manimala<sup>3</sup>
School of Mechanical and Aerospace Engineering, Oklahoma State University 201 General Academic Building, Stillwater, OK 74078

#### **ABSTRACT**

The thermoacoustic effect provides a means to convert acoustic energy to heat and vice versa without the need for moving parts. This is especially useful to construct mechanically-simple and robust energy harvesting devices, although there are limitations to the power-to-volume ratio achievable. The mechanical and thermal properties, as well as the geometry of the porous stack that forms a set of acoustic waveguides in thermo-acoustic devices, are key to its performance. In this study, we evaluate various additively manufactured polymer stacks against more conventional ceramic stacks using a benchtop thermos-acoustic refrigerator rig that uses Air at ambient pressure as its working fluid. The influence of parameters such as stack material, length, porosity, pore geometry, and location are examined using experiments in order to correlate with simulations using DeltaEC, a software tool based on Rott's linear approximation. Structure-performance relationships are established by extracting scaling laws for power-to-volume ratio and frequency-thermal gradient dependencies. It is found that additively manufactured stacks can deliver performance comparable to ceramic stacks while being more affordable and customizable for thermoacoustic transduction and multifunctional applications.

# 1. INTRODUCTION

The thermoacoustic phenomenon is manifested due to an instability caused by acoustic pressure waves propagating in a waveguide containing a fluid medium inducing oscillations in a porous stack, the ends of which are held under an imposed thermal gradient, thereby creating fluctuations in the rate of heat transfer. This, in turn, generates further pressure oscillations, leading to an unstable acoustic mode that can be harnessed without the need for any moving parts. Tracing their origins in early investigations by Rijke [1], Helmholtz [2], and Kirchhoff [3] studies to understand and apply thermoacoustics have been significantly expanded in recent times through the contributions of Rott

<sup>&</sup>lt;sup>1</sup> samarjith.biswas@okstate.edu

<sup>&</sup>lt;sup>2</sup> zackary.krawczyk@okstate.edu

<sup>&</sup>lt;sup>3</sup> james.manimala@okstate.edu

[4–6], Swift [7–9] and Tijani [10] among others. Thermoacoustic devices, which are broadly classified as heat engines or refrigerators, offer the advantage of having little to no moving parts and relatively quiet operation [11–14]. They can be operated in the standing or traveling wave modes. They have been used as an alternative to conventional prime movers to drive cryocoolers [15]. Thermoacoustic refrigerators have also been explored for sustainable cooling applications [16]. Traditionally, practical implementations of thermoacoustic devices have had challenges related to low efficiency [14, 17] and low power-to-volume ratio [18]. With current additive and hybrid fabrication materials and processes reaching commercial maturity, opportunities exist to utilize them to realize more affordable, lightweight, compact, and efficient components such as the stack for the next generation of thermoacoustic devices.

For the one-dimensional case, the thermoacoustic phenomenon in the linear regime is governed by Rott's approximation [5] which can be simulated using the software, DeltaEC [19]. A typical thermoacoustic refrigerator (TAR) consists of an acoustic waveguide or resonator equipped with an acoustic driver at one end and housing a porous structure called the stack across which the temperature gradient is established using hot (source-side) and cold-side heat exchangers. For the heat engine configuration, heat input is provided using the heat exchangers to generate acoustic waves that drive a prime mover in place of the acoustic driver. In addition to the design of the waveguide and selection of the working fluid, the stack plays a crucial role in the working of a TAR. The material properties and the geometric design of the stack in relation to the properties of the working fluid have key implications for the efficiency of the device.

There have been several studies on stacks for thermoacoustic devices in recent times. Yahya et al. [13] investigated the performance of 'random' stack materials in a standing wave device focusing on developing low-cost thermoacoustic refrigeration for domestic and commercial applications. Peng et al. [20] used a numerical approach to optimize the performance of stacks in a standing wave TAR. Alamir et al. [21] and Hariharan et al. [22] studied the influence of stack geometric parameters on the performance of TAR. Zolpakar et al. [23] investigated a specific 3D printed stack for use in TARs. It was found that temperature gradients of around 15 °C can be established. Alcock et al. [24] experimentally studied the influence of ceramic stack parameters on the performance of TAR to extract guidelines for the optimal design of such stacks. A comparative study of various heat exchanger geometries for stacks was conducted by Piccolo et al. [25].

In this study, various additively manufactured (AM) stacks are evaluated against more conventional ceramic stacks using experiments to gauge the influence of material and geometric parameters on their performance. The potential of utilizing the versatility provided by additive and hybrid fabrication process to develop innovative stack geometries could enable practical solutions for more efficient thermoacoustic devices, especially for multifunctional applications.

### 2. MATERIALS AND METHODS

An experimental parametric study is conducted on ceramic and AM stacks using a benchtop thermoacoustic test rig. Details of the experimental setup, design, and fabrication of the test stacks and the test cases investigated are presented.

## 2.1. Experimental Setup

A benchtop thermoacoustic test rig shown in Figure 1 was constructed to evaluate the stacks. The test rig consists of an acrylic tube waveguide equipped with an acoustic driver (speaker) at one end and capped using a hard rubber end-stop at the other end. The waveguide has a length of 1524 mm and a diameter of 101 mm. The test stack can be positioned at a specific location along the axis of the tube. A function generator coupled with a signal conditioner and amplifier are used to provide the input excitation for the 50 W speaker. K-type digital thermocouples with a resolution of 0.1 °C placed at the source and receiver sides of the stack are used to measure the hot and cold-side temperatures, respectively. Microphones with a resolution of 0.1 dB are used to verify the source and receiver-side sound pressure levels. A DAQ computer is used to record all data. The acoustic excitation is applied at discrete frequencies within the frequency range of interest that spans the fundamental

resonance frequency of the tube. For all tests, the sound pressure level was maintained at about 128 dB as measured under steady-state conditions within the tube. The entire tube assembly is wrapped in insulating foam during testing in order to minimize thermal and acoustic flanking paths.

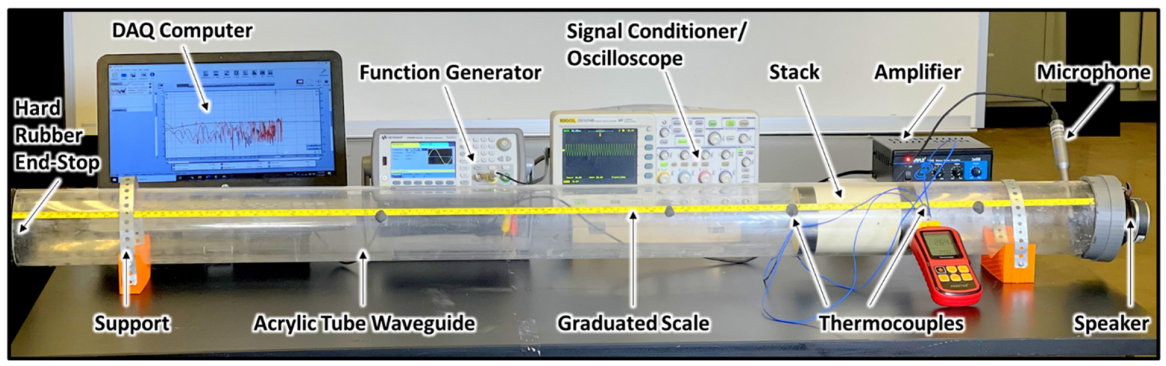


Figure 1: Thermoacoustic refrigerator test rig.

A schematic depiction of the test rig denoting the experimental parameters is shown in Figure 2. Air under ambient conditions ( $P_m = 1 \text{ atm}$ ,  $T_m = 21 \,^{\circ}\text{C}$ ) is used as the working fluid. The influence of parameters related to acoustic excitation and stack material, geometry, and position on the thermoacoustic temperature gradient across the stack are explored using experiments. The fundamental resonant frequency of a standing wave tube with a closed end can be computed using the relation,

$$f_o = \frac{c}{2L_s'} \tag{1}$$

Accounting for the effective length of the tube,  $L'_s$ , this gives a theoretical fundamental resonance frequency of 114.5 Hz under ambient conditions for the test rig, which is suitable to investigate thermoacoustic transduction at relatively low frequencies using AM stacks for potential applications related to energy harvesting.

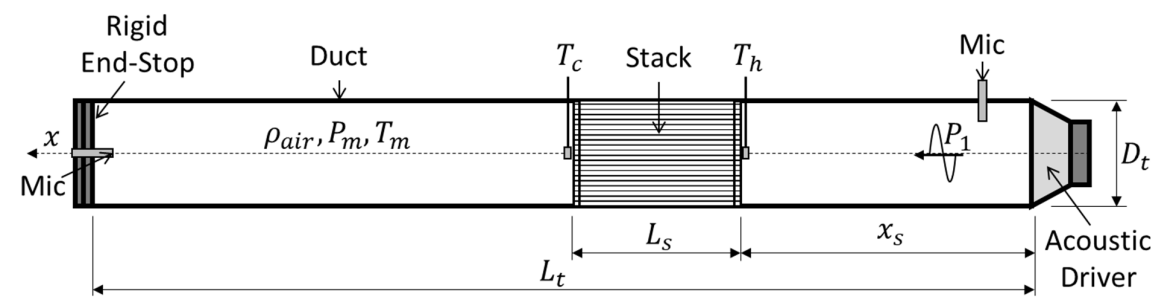


Figure 2: Schematic depiction of experimental parameters.

## 2.2. Stacks

The efficiency of a stack for a chosen working fluid is dependent upon its pore geometry. In this context, the thermal and viscous penetration depths [26] of the working fluid (air under ambient conditions in this case) play an important role. The thermal and viscous penetration depths for air are given by

$$\delta_k = \sqrt{\frac{2k}{\omega \rho c_p}} \tag{2}$$

$$\delta_{v} = \sqrt{\frac{2\mu}{\omega\rho}} \tag{3}$$

where k is thermal conductivity,  $\omega=2\pi f$  is the angular frequency,  $\rho$  is density,  $c_p$  is specific heat and  $\mu$  is the dynamic viscosity of the working fluid. Now, for air under ambient conditions, k=0.026 W/(m.K);  $\rho=1.176$  kg/m³;  $c_p=1000$  J/(kg.K); and  $\mu=1.87\times 10^{-5}$  kg/(s.m). For a resonance frequency of  $f=f_0=115$  Hz, the thermal and viscous penetration depths are computed to be

$$\delta_k = 0.247 \, mm, \quad \delta_v = 0.227 \, mm$$
 (4a, b)

Apart from a large area of contact between the working fluid and the stack surfaces and thinner thermal and viscous boundary layers, stack wall (plate) separation,  $2y_0$  should be on the order of two to four times the thermal and viscous penetration depths so as to ensure that the thermoacoustic cycle is effective. Therefore, stack wall separations in the range of 0.5 to 1 mm are desirable in this case.

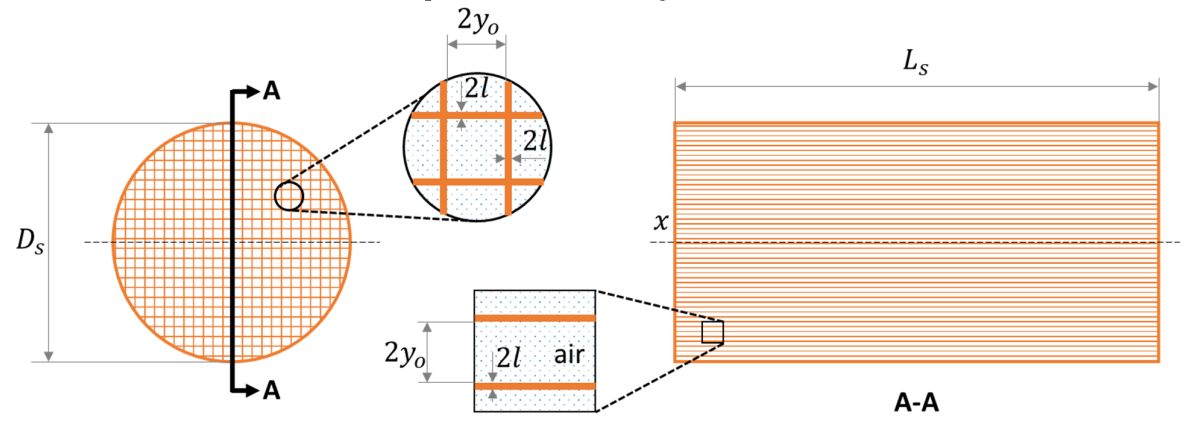


Figure 3: Diagram showing geometric parameters of a stack.

Table 1: Summary of ceramic and additively manufactured stack properties.

Property	CE170P80	CE178P85	PLA100P64	RES100P64	ASA100P64	PLA170P64	PLA100P44
Length, $L_s$ , mm	170	178	100	100	100	170	100
Diameter, $D_s$ , mm	97	76.2	76.2	100	101	101	101
Areal porosity, $\phi$	0.80	0.85	0.64	0.64	0.64	0.64	0.44
Pore wall thickness, 2 <i>l</i> , mm	0.101	0.101	0.50	0.50	0.50	0.50	0.50
Pore width, 2 <i>y</i> <sub>0</sub> , mm	0.861	1.20	2	2	2	2	1
Material	Ceramic	Ceramic	PLA	Resin	ASA	PLA	PLA

The material properties of the stack also play a significant role in the performance of the thermoacoustic refrigerator and engine. In order to maintain a steady-state temperature gradient along the stack plates, the stack material should have a higher heat capacity than the working fluid [26]. An optimal thermal conductivity also helps establish the requisite temperature gradient along the axial direction of the stack. A minimal pore wall thickness (2l) for the stack material enables creating a higher areal porosity. Stacks with thicker pore walls also tend to create eddies at the corner, which contribute to dissipative loss [27]. Various ceramic and additively manufactured (AM) stacks are considered for testing. Their details are summarized in Table 1. The ceramic stacks are sourced commercially from Corning's Celcor® line of filters and substrates, which are commonly used as con-

ventional stacks for thermoacoustic devices [28]. These are manufactured through an extrusion process and can be obtained with different combinations of lengths, diameters, and pore geometry. For the present study, two ceramic substrates of lengths around 170 mm and areal porosity of about 0.8 are chosen to act as the baseline stacks. For the AM stacks, commonly used polymeric materials and processes are considered. Three materials – Polylactic Acid (PLA), Formlabs standard resin, and Acrylonitrile Styrene Acrylate (ASA) are considered. The material properties of the stacks are summarized in Table 2. The properties for ceramic stack are estimated whereas those for the AM stacks are specified by the manufacturers.

Table 2: Material properties of stacks.

Stack	Material	Layer Height (µm)	Thermal Conductivity (W/m K)	Heat capacity (J/kg·°C)	Melting Point (°C)	Density (kg/m³)	Modulus of Elas- ticity (GPa)	Pois- son's Ratio
CE170P80	Ceramic	-	>1.5	352	>2000	2000- 6000	>200	0.27
CE178P85	Ceramic	-	>1.5	352	>2000	2000- 6000	>200	0.27
PLA100P6	PLA	100	0.13	1800	173	1240	3.5	0.3
PLA100P4	PLA	100	0.13	1800	173	1240	3.5	0.3
PLA170P64	PLA	100	0.13	1800	173	1240	3.5	0.3
ASA100P64	ASA	100	0.175	1300	135	1050	2.2	0.39
RES100P64	Resin	50	0.2	1000-1300	176	1250	2.7	0.35

PLA and ASA test stacks are fabricated using the Fused Deposition Modeling (FDM) process, and the resin test stack is fabricated using the stereolithographic process. The lengths and porosity of the AM stacks are chosen as detailed in Table 2 to investigate the influence of these parameters. It is noted that while the AM processes chosen are affordable, they do also impose restriction on the geometry and size of the pore structure that can be fabricated. All test stacks considered in this study have square cross-sections for their pore, but the pore wall thickness for the ceramic stacks (0.1 mm) are much smaller than those for the AM stacks (0.5 mm). Photographs of the ceramic and AM stacks are shown in Figure 4.



Figure 4 : (a) Photographs of various ceramic and AM stacks and (b) Porous structure of an AM stack.

## 2.3. Test Cases

The experimental test cases are summarized in Table 3. Test cases are considered to evaluate the influence of parameters such as time to steady-state, acoustic excitation frequency, stack length, porosity, material, and position. For each case, the base parametric setting ( $[P_m, T_m, P_1] = [1 \text{ atm}, 21 \, ^{\circ}\text{C}, 128 \, dB]$ ) is preserved. Except for the stack position variation cases, all other cases have a stack position,  $x_s = 100 \, mm$ . Multiple trials are considered for various cases, and in each case, the cold and hot side temperatures are recorded for discrete excitation frequencies spanning the frequency range of interest (80-140 Hz).

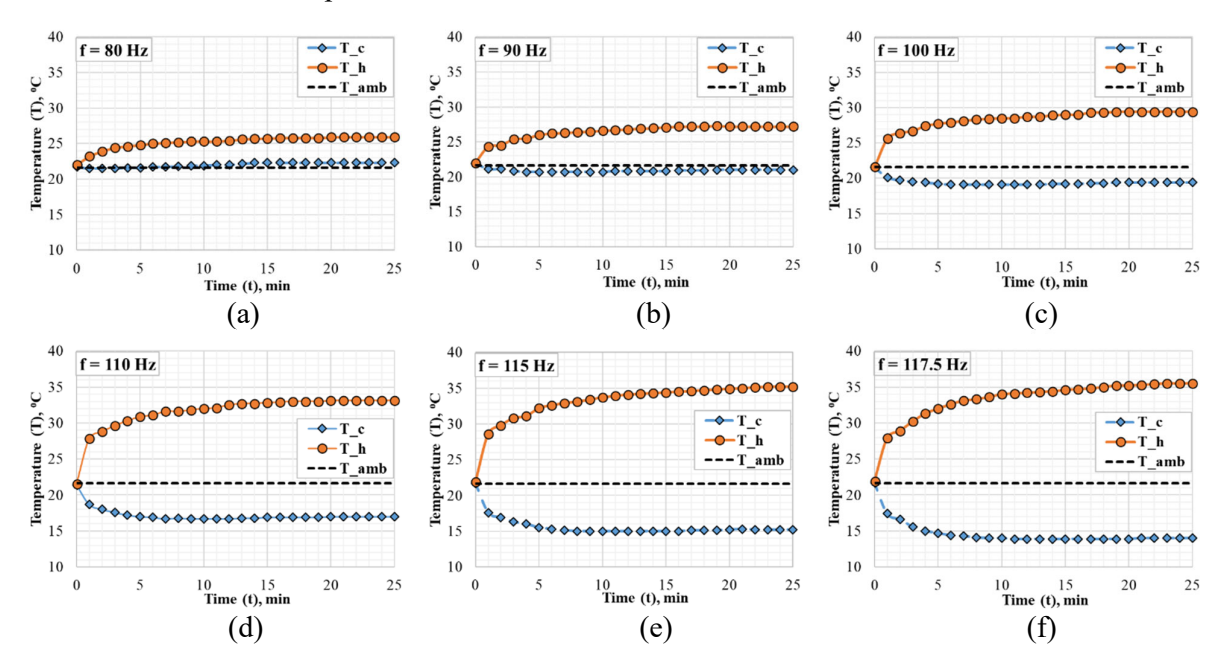
Table 3: Summary of experimental test cases.

Case #	Parameter	Values/ Type	Stacks	Measurements
t1-t4	Time to steady-state	$t \in [0, 45]min$	CE170P80 PLA170P64 PLA100P44 ASA100P64	$T_c, T_h, P_1, t, f$
f1-f7	Excitation frequency	$f \in [80,140]Hz$	All	$T_c, T_h, P_1, f$
L1, L2	Stack length	L = [100, 170] mm	PLA100P64 PLA170P64	$T_c, T_h, P_1, f$
φ1, φ2	Stack porosity	$\phi = [0.64, 0.44]$	PLA100P64 PLA100P44	$T_c, T_h, P_1, f$
M1-M5	Stack material	Ceramic PLA ASA Resin	CE170P80 PLA170P64 PLA100P64 ASA100P64 RES100P64	$T_c, T_h, P_1, f$
x1-x7	Stack position	$x_s = [100, 200, 300] mm$	All	$T_c, T_h, P_1, f_o$

## 3. DISCUSSION OF RESULTS

# 3.1. Time to Steady-State

The evolution of the cold and hot-side temperatures to steady-state for the ceramic stack CE170P80, at various acoustic excitation frequencies is shown in Figure 5. Several features of interest are observed. Away from resonance, it is noted that the gradient is established predominantly due to the hot-side temperature rising above ambient temperature and less so due to the cold-side temperature falling below ambient. As the excitation frequency approaches closer to resonance, the rise in hot-side temperature is still larger than the drop in the cold-side temperature. However, the drop in the cold-side temperature is now significantly larger than at non-resonant frequencies. In general, the convergence to steady-state is found to be faster for the cold-side compared to the hot-side as well as for ceramic stacks in comparison to the AM stacks.



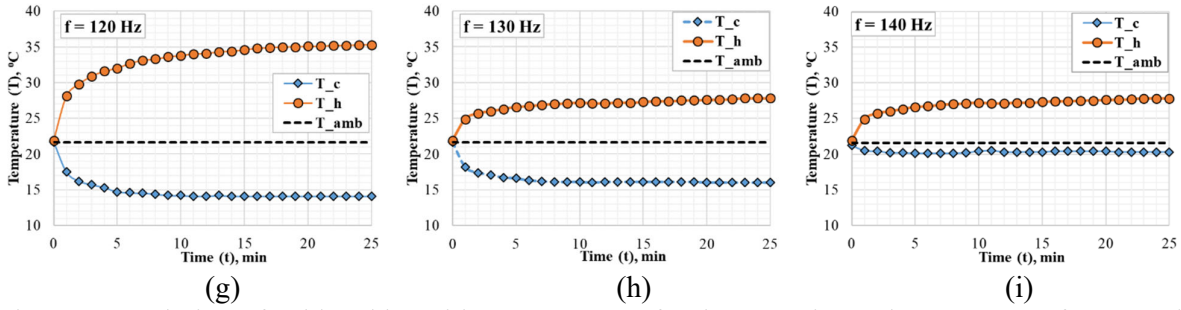


Figure 5: Evolution of cold and hot-side temperatures for the ceramic stack, CE170P80 for acoustic excitation frequencies of (a) 80, (b) 90, (c) 100, (d) 110, (e) 115, (f) 117.5, (g) 120, (h) 130 and (i) 140 Hz.

# 3.2. Excitation Frequency

The steady-state temperature difference between hot and cold sides ( $\Delta T$ ) and the Carnot coefficient of performance for all stacks versus excitation frequency are shown in Figure 6. The stack position was retained at 100 mm for these cases. It can be seen that the temperature difference peaks in the frequency range of 110-120 Hz, with the peak value being obtained at 115 or 117.5 Hz. This corresponds very well with the theoretically computed resonance frequency for the thermoacoustic rig (114.49 Hz). In general, the AM stacks have comparable or better performance than the ceramic stacks considered. It is noted that while the ceramic stacks have higher porosity than the AM stacks, the diameter of the CE175P85 stack is markedly smaller than the diameter of the waveguide, which can explain its lower performance. Among the AM stacks, the resin and ASA stacks perform better than the PLA stacks. The maximum temperature difference ( $\Delta T = 24.8$  °C) and the corresponding maximum Carnot efficiency (0.653) are obtained for the resin stack at an excitation frequency of 117.5 Hz. The resin stack is not the longest nor does it have the best geometric parameters for its pores. However, it was observed that its surface finish seems to be the best among all the stacks, potentially minimizing dissipative effects. Overall, AM stacks have the potential to deliver the same performance as more conventional ceramic stacks while being more affordable, potentially lightweight, and amenable to more complex geometries, which could be useful to improve the power-tovolume ratio of thermoacoustic devices.

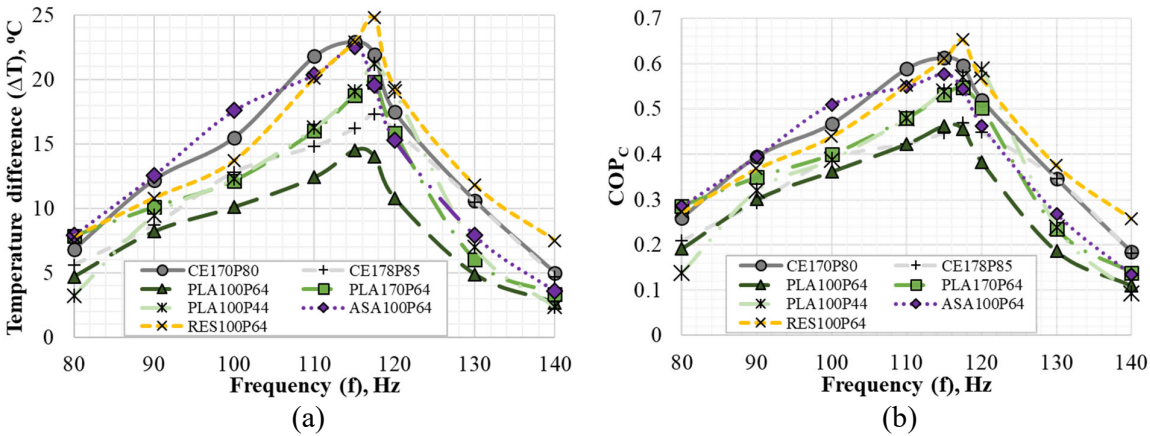


Figure 6: (a) Steady-state temperature difference between hot and cold sides and (b) coefficient of performance versus excitation frequency for ceramic and AM stacks. The stack position was set at  $L_s = 100 \ mm$ .

#### 3.3. Stack Length

For PLA stacks of the same porosity, the comparison of the performance versus frequency for two variants having different (100 and 170 mm) lengths is shown in Figure 7. The longer stack performs better over the entire frequency range of interest with an increase in temperature difference of around 40% near resonance. A longer stack length tends to reduce the heat conducted through the

stack walls between the hot and cold sides as well as the traverse distance of the air parcel. When dissipative effects are small, this is seen to establish a higher temperature gradient between the hot and cold sides.

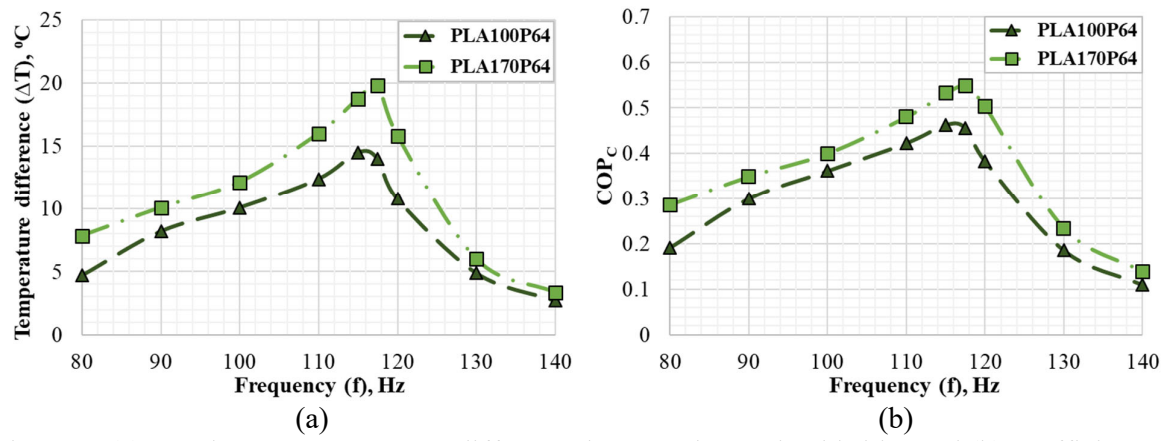


Figure 7: (a) Steady-state temperature difference between hot and cold sides and (b) coefficient of performance versus frequency for PLA stacks of different lengths but same porosity. The stack position was set at  $L_s = 100 \ mm$ .

### 3.4. Stack Porosity

Comparing the influence of stack porosity for PLA stacks of the same length in Figure 8, it can be seen that the lower porosity (0.44), in this case, results in about a 50% increase in the temperature difference at resonance. Note that the lower porosity for PLA100P44 is realized by reducing the pore width but retaining the pore wall thickness the same as that for PLA100P64 as opposed to scaling both the width and wall thickness. This is due to the restriction posed by the additive manufacturing processes chosen. Therefore, although the porosity is lower for the P44 stack, its pore width of 1 mm is closer than that of the P64 stack (2 mm) to the two to four times the thermal penetration depth which is recommended for the effectiveness of the stack.

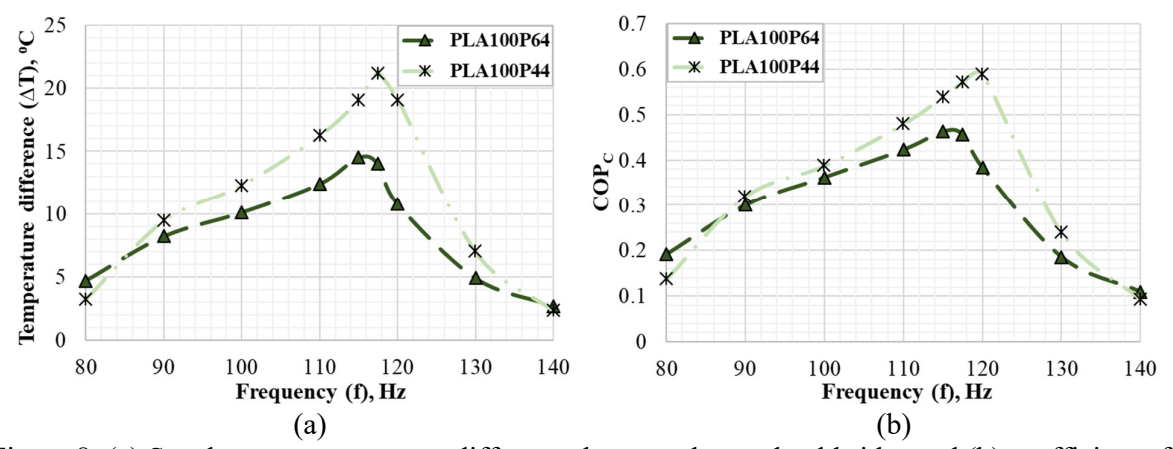


Figure 8: (a) Steady-state temperature difference between hot and cold sides and (b) coefficient of performance versus frequency for PLA stacks of different porosity but same lengths. The stack position was set at  $L_s = 100 \ mm$ .

# 3.5. Stack Material

Among the AM stacks of the same length and porosity, the resin stack is found to perform the best, as seen in Figure 9. ASA stack has similar performance prior to resonance, but it drops below the resin stack above resonance. The performance of the PLA stack is markedly lower. As noted before, the resin stack has the best surface finish amongst the AM stacks, while the PLA stack has a relatively poor finish which could influence the dissipative effects. Also, the AM stacks, in general, have a higher heat capacity than the working fluid (air) which is desirable. For the ceramic stacks,

the porosity is higher due to the pore wall thicknesses being significantly lower than those for the AM stacks. Transitioning to AM processes that enable thinner pore wall thicknesses could result in improved performance for AM stacks.

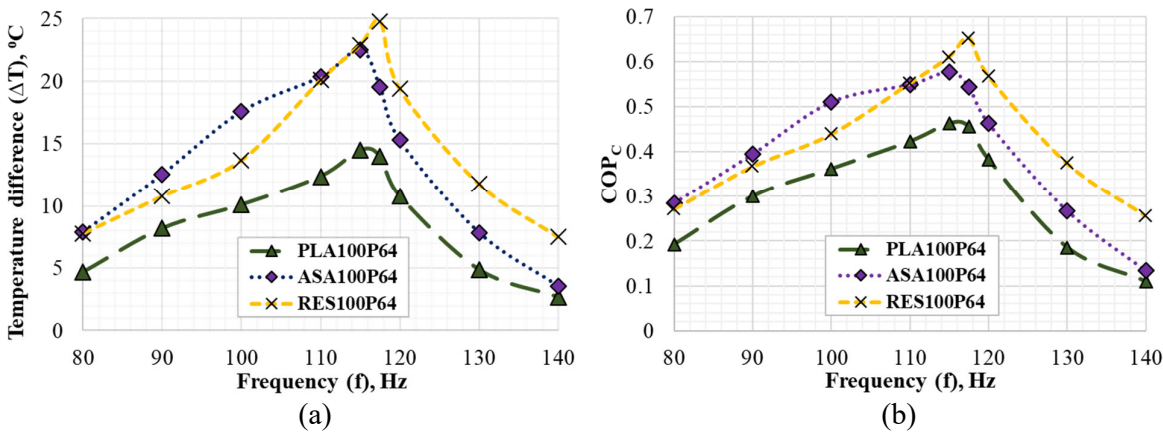


Figure 9: (a) Steady-state temperature difference between hot and cold sides and (b) coefficient of performance versus frequency for AM stacks of different material but same length and porosity. The stack position was set at  $L_s = 100 \ mm$ .

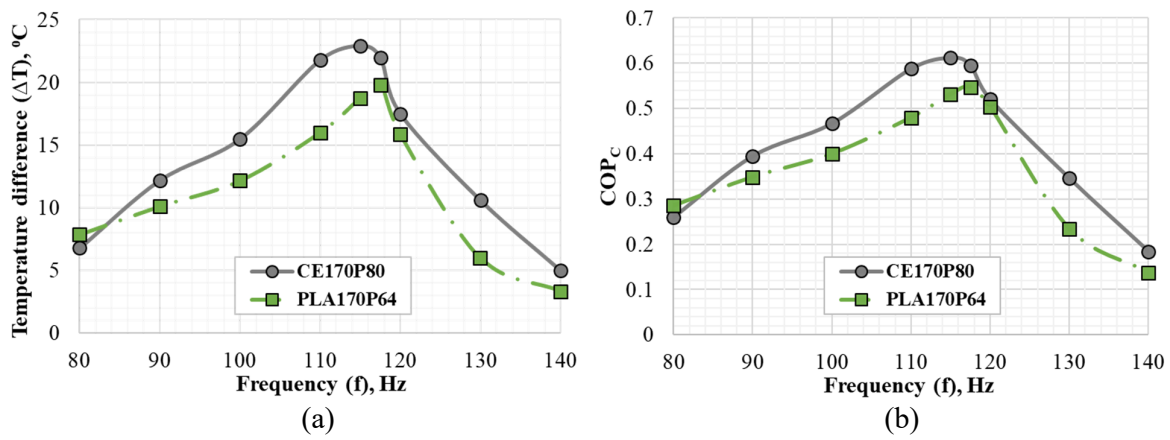


Figure 10: Comparison of (a) steady-state temperature difference between hot and cold sides and (b) coefficient of performance versus frequency for ceramic and PLA stacks of the same length. The stack position was set at  $L_s = 100 \ mm$ .

#### 3.6. Stack Position

The location of the test stack within the waveguide is altered in order to change the stack position,  $x_s$ . For each case, the performance is recorded at an excitation frequency corresponding to the resonance (117.5 Hz), as shown in Figure 11. It is observed that, in general, the performance drops as the distance from the source is increased. Depending on the dimensions of the acoustic waveguide, which determines the wavelength at resonance, interactive effects are generated when the position of the stack is changed along the axis of the tube. The gradient of the drop in performance with stack position is seen to be lower for the ceramic stacks than those for AM stacks. While the resin stack had the best performance for a stack position closest to the source, it drops considerably (nearly 50%) as the stack is moved farther away. Placing the stack extremely close to the driver could potentially trigger nonlinear effects which need to be investigated further.

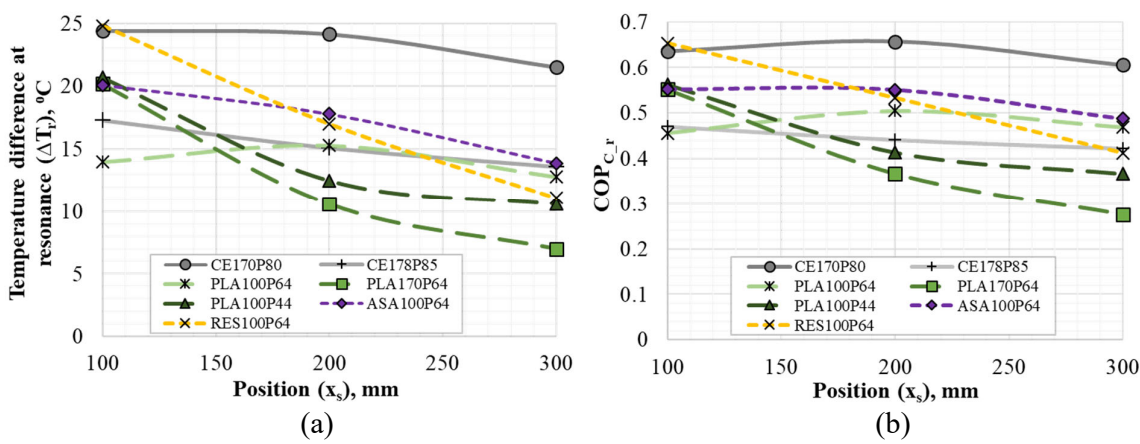


Figure 11: (a) Steady-state temperature difference between hot and cold sides and (b) coefficient of performance versus stack position at an excitation frequency of 117.5 Hz (resonance) for ceramic and AM stacks.

## 3.7. Estimation of Error

Error bounds estimated from multiple trials for the evolution of the cold and hot-side temperatures to steady-state for the ceramic stack CE170P80, and the propagated error bounds for the steady-state temperature difference for ceramic and AM stacks are shown in Figure 12. The trials account for stack setup, data transduction, and initial condition induced errors. Overall, the maximum error on the temperature measurement is within 1.5% for the ceramic stack, and the maximum error for the temperature difference for the ceramic and AM stacks is 15% (although errors for most data points are significantly smaller). The error bounds for the other cases are typically within these maximum values.

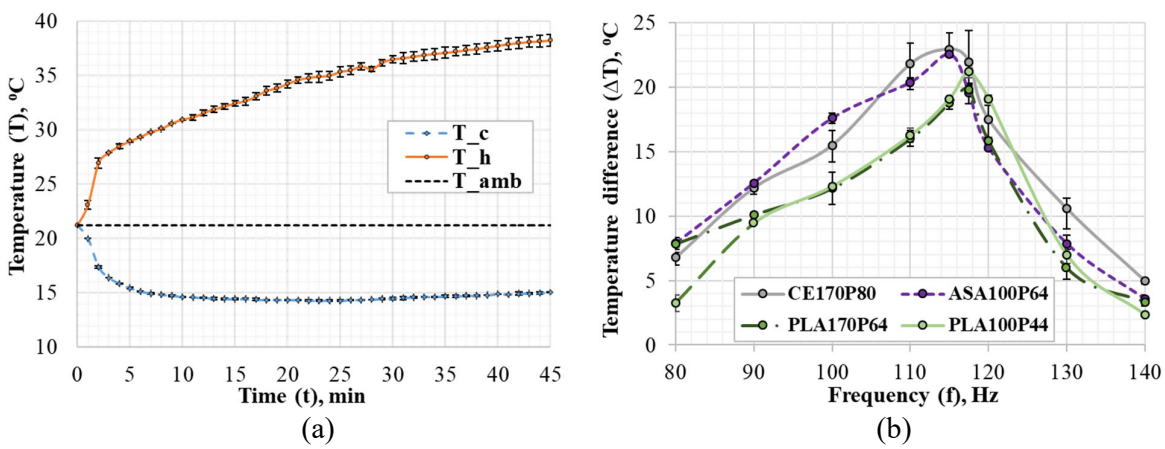


Figure 12: Error bounds for (a) cold and hot-side temperatures versus time for ceramic stack, CE170P80 and (b) steady-state temperature difference between hot and cold sides versus excitation frequency for ceramic and AM stacks. The stack position was set at  $L_s = 100 \ mm$ .

# 4. CONCLUSION

An experimental parametric study was conducted to evaluate various additively manufactured stacks against more conventional ceramic stacks using a benchtop thermoacoustic rig. The influence of parameters such as time to steady-state, excitation frequency, stack material, length, porosity, and position on the efficiency are examined. A benchtop thermoacoustic test rig was constructed to test the stacks in refrigerator mode. It is found that the hot and cold-side temperatures evolve to steady-state under 25 minutes, with the rate of convergences being faster for the cold-side as well as for the ceramic stacks. The temperature gradient and efficiency are found to peak between acoustic excitation frequencies of 115 and 120 Hz. Among all cases, the resin stack showed the largest temperature

gradient of about 24.8 °C at 117.5 Hz. Stack positions close to the source are found to be more efficient. In general, the performance of AM stacks is found to be comparable to the ceramic stacks, although several of the parameters involved could be further optimized. Further studies are currently underway to correlate with DeltaEC simulations in order to develop innovative stack geometries that improve efficiency and power-to-volume ratio for thermoacoustic devices for multifunctional applications.

#### 5. ACKNOWLEDGEMENTS

Support from NSF RII Track-4 Grant No. 2033399 is gratefully acknowledged. Thanks are due to graduate student Oluwafemi Akinmolayan for help with the experiments.

## 6. REFERENCES

- 1. Rijke, P. L. Notiz Über Eine Neue Art, Die in Einer an Beiden Enden Offenen Röhre Enthaltene Luft in Schwingungen Zu Versetzen. *Annalen der Physik und Chemie*, **183(6)**, 339–3431 (1859).
- 2. Heidelberg, N. Zu. Verhandlungen Des Naturhistorisch-Medizinischen Vereins Zu Heidelberg. Naturhistorisch-Medizinischen Vereins zu Heidelber, Naturhistor.-Med. Verein, (1965)
- 3. Kirchhoff, G. On the Influence of Heat Conduction in a Gas on Sound Propagation. *Annual Review of Physical Chemistry*, **134**, 177–193, (1868).
- 4. Rott, N. Thermoacoustics. Advances in Applied Mechanics, 20, 135–175, (1980).
- 5. Rott, N. Damped and Thermally Driven Acoustic Oscillations in Wide and Narrow Tubes. *Zeitschrift für angewandte Mathematik und Physik ZAMP*, **20(2)**, 230–243, (1969).
- 6. Rott, N. & Zouzoulas, G. Thermally Driven Acoustic Oscillations, Part IV: Tubes with Variable Cross-Section. *Journal of Applied Mathematics and Physics*, **27(2)**, 197–224, 1976.
- 7. Swift, G. W. Analysis and Performance of a Large Thermoacoustic Engine. *The Journal of the Acoustical Society of America*, **92(3)**, 1551–1563, (1992).
- 8. Backhaus, S., and Swift, G. W. A Thermoacoustic-Stirling Heat Engine: Detailed Study." *The Journal of the Acoustical Society of America*, **107**, 1145, (2000).
- 9. Gardner, D.L., & Swift, G.W. A Cascade Thermoacoustic Engine. *Journal of Acoustic Society of America*, **114**, 1905–1919, (2003).
- 10. Tijani, M. Loudspeaker-Driven Thermo-Acoustic Refrigeration. *Phd Thesis, Technische Universiteit Eindhoven*, (2001).
- 11. Paek, I., Braun, J.E. & Mongeau, L. Evaluation of standing-wave thermoacoustic cycles for cooling applications. *International Journal of Refrigeration*, **30**, 1059–1071 (2007).
- 12. Raut, A.S. & Wankhede, U.S. Review of investigations in Eco-Friendly thermoacoustic refrigeration system. *Thermal Science*, **21**, 1335–1347 (2017).
- 13. Yahya, S.G., Mao, X. & Jaworski, A.J. Experimental Investigation of Thermal Performance of Random Stack Materials for use in Standing Wave Thermoacoustic refrigerators. *International Journal of Refrigeration*, **75**, 52–63 (2017).
- 14. Jin, T., Huang, J., Feng, Y., Yang, R., Tang, K., and Radebaugh, R. Thermoacoustic Prime Movers and Refrigerators: Thermally Powered Engines without Moving Components. *Energy*, **93**, 828–853 (2015).
- 15. Setiawan, I., Achmadin, W. N., Murti, P. & Nohtomi, M. Experimental Study on a Standing Wave Thermoacoustic Prime Mover with Air Working Gas at Various Pressures. *Journal of Physics: Conference Series*, **710(1)**, (2016).
- 16. Hamood, A., Jaworski, A. J. & Mao, X. Development and Assessment of Two-Stage Thermoacoustic Electricity Generator. *Energies*, **12(9)**, 1-18, (2019).
- 17. Swift, G.W. Thermoacoustics. *Acoustical Society of America*, (2017).
- 18. Alcock, A. C., Tartibu, L. K., & Jen, T. C. Design and Construction of a Thermoacoustically Driven Thermoacoustic Refrigerator. *Proceedings of the Conference on the Industrial and Commercial Use of Energy, ICUE*, 1–7, (2017).
- 19. Clark, J. P., Ward, W. C. & Swift, G. W. Design Environment for Low-Amplitude Thermoacoustic Energy Conversion (DeltaEC). *The Journal of the Acoustical Society of America*, **122(5)**, 3014, (2010).
- 20. Peng, Y., Feng, H. & Mao, X. Optimization of Standing-Wave Thermoacoustic Refrigerator Stack

- using Genetic Algorithm. International Journal of Refrigeration, 92, 246–255, (2018).
- 21. Alamir, M. A. Experimental Study of the Stack Geometric Parameters Effect on the Resonance Frequency of a Standing Wave Thermoacoustic Refrigerator Frequency of a Standing Wave Thermoacoustic Refrigerator. *International Journal of Green Energy*, **16(8)**, 639–651, (2019).
- 22. Hariharan, N. M., Sivashanmugam, P., and Kasthurirengan, S. Influence of Stack Geometry and Resonator Length on the Performance of Thermoacoustic Engine. *Applied Acoustics*, **73(10)**, 1052–1058, (2012).
- 23. Atiqah, N., Mohd-ghazali, N., Ahmad, R. & Maré, T. Performance of a 3D-printed stack in a standing wave thermoacoustic refrigerator. *Energy Procedia*. *105*, 1382–1387 (2017).
- 24. Alcock, A.C., Tartibu, L.K. & Jen, T.C. Experimental Investigation of Ceramic Substrates in Standing Wave Thermoacoustic Refrigerator. *Procedia Manufacturing*, 7, 79–85 (2017).
- 25. Piccolo, A., Siclari, R., Rando F. & Cannistraro, M. Comparative performance of thermoacoustic heat exchangers with different pore geometries in oscillatory flow. Implementation of experimental techniques. *Applied Science*, 7, (2017).
- 26. Tijani, M.E.H., Zeegers, J.C.H. & De Waele, A.T.A.M. Design of thermoacoustic refrigerators. Cryogenics, **42**, 49–57 (2002).
- 27. Tasnim, S.H. Porous Media Thermoacoustic Stacks: Measurements and Models. *Ph.D. thesis, University of Waterloo* (2011).
- 28. Ryan, T.S. Design and Control of a Standing Wave Thermoacoustic Refrigerator. *Master's thesis, University of Pittsburgh* (2006).